PROCEEDINGS, 48th Workshop on Geothermal Reservoir Engineering
Stanford University, Stanford, California, February 6-8, 2023
SGP-TR-224

Calibration Parameters Required to Match the Utah FORGE 16A(78)-32 Stage 3 Stimulation with a Planar Fracturing Model

Mark McClure

ResFrac Corporation

mark@resfrac.com

Keywords: Utah FORGE, EGS, numerical modeling, hydraulic stimulation

ABSTRACT

Enhanced Geothermal Systems (EGS) use hydraulic stimulation to improve production from high temperature, relatively low permeability formations. EGS projects are usually performed in crystalline lithologies, such as granite. In these settings, there is ambiguity about the relative role of newly forming and preexisting fractures, and there is significant uncertainty about the input parameters that should be used in numerical models. The uncertainties can only be resolved by gathering of field-scale data, and then evaluating modeling approaches and input parameters based on their ability to rationalize the observations. This paper analyzes the data from the Stage 3 stimulation of Well 16A(78)-32 at the Utah FORGE project. The stimulation was performed in granitic rock, from a single perforated interval, with cross-linked gel and microproppant. High-resolution microseismic observations show that the stimulation formed a planar region perpendicular to the minimum principal stress, suggesting that a planar fracture model is appropriate for describing the stimulation. The microseismic observations constrain the size, direction, and aspect ratio of fracture. Hydraulic fracture propagation in granitic rock poses novel theoretical questions. Because granitic formations lack layering and should be relatively homogeneous (compared with sedimentary formations), fracture propagation models may tend to predict extreme vertical height growth; however, this is not observed in actual data. The 16A(78)-32 Stage 3 data suggests that the fracture propagated slightly more laterally than vertically, and with only a modest upward bias. In this paper, a planar fracture model is built and calibrated to match the data. To match the observed fracture geometry with a fracturing simulator, an automated history matching algorithm was used to vary five field-scale calibration parameters that affect fracture geometry. The algorithm converged to a relatively narrow combination of parameters to match the data. The match implies: (a) modestly elevated toughness above typical laboratory values, (b) substantial 'pressure dependent permeability' contributing to leakoff from the main fracture, (c) moderately decreased fracture conductivity from the standard cubic law, (d) moderate anisotropy of vertical toughness, and (e) modest anisotropy of vertical conductivity. Future stimulations at Utah FORGE will provide opportunities to evaluate and/or refine the model parameters derived from the Stage 3 match.

1. INTRODUCTION

1.1 Background

The Utah FORGE project (Frontier Observatory for Research in Geothermal Energy) is a field demonstration project testing the application of multistage hydraulic stimulation along highly deviated laterals for Enhanced Geothermal Systems (EGS) development (Moore et al., 2019; McLennan et al., 2023). An injection well 16A(78)-32 was drilled from October 2020 to January 2021 (Samuel et al., 2022). In April 2022, the first three stages of the well were stimulated. The first stage, at the toe of the well, was left openhole. The second and third stages were cased and perforated. The wellbore configuration is shown in Figure 1 (reproduced from Xing et al., 2022).

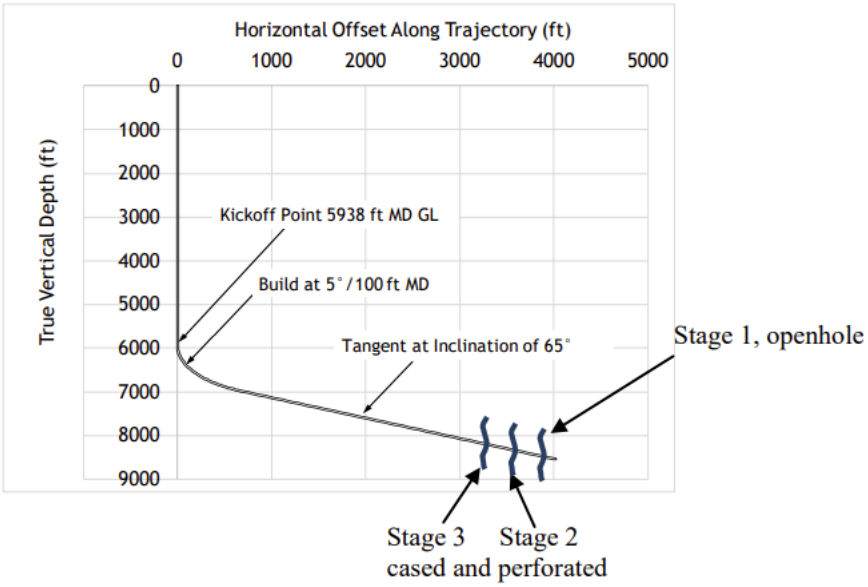

Figure 1: Schematic of the 16A(78)-32 wellbore trajectory. Figure reproduced from Xing et al. (2022).

Conventionally, Enhanced Geothermal Systems (EGS) have been designed with near vertical wells and long openhole sections. They have been stimulated with a 'bullheading' procedure, where fluid is injected into the entire wellbore without any mechanical isolation into separate stages. Two ongoing projects – Utah FORGE and a project by Fervo Energy (Norbeck et al., 2023; Fercho et al., 2023) – are the first to test the application of multistage stimulation along a highly deviated wellbore in crystalline rock for EGS.

Past EGS has been affected by flow localization, where fluid exits the well from a relatively small number of locations along the wellbore (Evans et al., 2005). The Utah FORGE and Fervo projects are planning to overcome flow localization with plug and perf completion techniques developed by the petroleum industry. Multistage stimulation uses plugs or other forms of mechanical isolation to sequentially inject into sections of the well, called stages. Within each stage, perforation pressure drop is used to force fluid from as many as 15-20 perforation clusters, creating a relatively uniform distribution of flow (Cramer, 1987; Lorwongngam et al., 2020). Shale core-through studies show that this technique generates a high number of densely spaced, mostly parallel hydraulic fractures (Raterman et al., 2019; Gale et al., 2022). Remarkably, core-through studies suggest that opening mode hydraulic fractures are generated on average once every few feet, evidently propagating in fracture swarms, forming thousands of fractures along a typical 10,000 ft lateral. These results are encouraging for EGS because the generation of numerous closely spaced fractures through a large volume of rock is precisely what is needed to achieve economic performance and long-term sustainability (Doe and McLaren, 2016; Li et al., 2016).

In shale, core-through studies in shale have led to a paradigm shift in our understanding of hydraulic stimulation. At the outset of the shale revolution, it was hypothesized that injection created a 'complex network of fractures,' involving abundant stimulation of preexisting natural fractures in a zig-zagging network for flow (Weng et al., 2011). But as described by Gale et al. (2022), "Sealed natural fractures are present in the core but apparently play a limited role in causing hydraulic fracture complexity with fewer than 10% natural fractures reactivated by hydraulic fracturing. Bedding plane reactivation due to hydraulic fracturing is also limited in the volume of core observed." Instead, they note "Observations of hydraulic fracture morphology indicate that diversion, bifurcation, and segmentation may account for the large number of fractures observed," as the fracture strands cluster into swarms. Fiber-optic and image log observations in offset wells are also consistent with this conceptual model, as they show fractures propagating in largely linear and parallel bands in each stage (Ugueto et al., 2021).

It is unclear whether these findings from shale are transferrable to EGS projects in granitic or volcanic rocks, such as Utah FORGE. Unfortunately, without direct observations such as core, fiber, or imaging logs in offset wells, it is difficult or impossible to conclusively assess what are the dominant 'mechanisms of stimulation' and what are the geometries of the flow pathways during stimulation and circulation.

McClure and Horne (2014) reviewed EGS experiences to-date and concluded that opening mode hydraulic fractures have formed at the great majority of historic EGS projects. They argued that stimulation mechanism depends on whether large, preexisting, naturally permeable fault zones are present in the formation. If they are present, then fluid will tend to divert into these features (as has been documented at the Soultz project, for example, by Evans et al., 2005). If they are not present, then fluid will tend to localize into newly forming hydraulic fractures. They argued that during injection into openhole sections, newly forming hydraulic fractures use natural fractures as nucleation sites, creating the observation that fluid is exiting the well from natural fractures, even though hydraulic fracture propagation is occurring in the far-field. In fact, this process appears to have been observed at the EGS Collab project (Fu et al., 2021). Inspired by concepts from the shale industry, McClure and Horne (2014) hypothesized that the 'complex fracture network' process described by Weng et al. (2011) might create branching networks, from the interaction of the hydraulic fractures with natural fractures. However, as discussed above, more recent observations from shale suggest that fracture tend to form in swarms of subparallel opening

mode fractures, and the conceptual model of a branching DFN dominated by natural fractures is not representative of most stimulations. Thus, it is a plausible – but unproven – hypothesis that stimulation in crystalline rock might generate similar swarms of subparallel hydraulic fractures.

The mechanism of stimulation is very likely to be influenced by the stimulation strategy. If injecting into lengthy openhole sections, as in conventional EGS designs, it is more likely that fluid will encounter permeable natural fractures and divert into them. However, in plug and perf completions, fluid must exit the casing at discrete, regularly spaced intervals. It is unlikely that a particular perforation cluster will coincide with a permeable natural fracture, and so it is likely that one or more opening mode tensile fractures will be forced to initiate at the wellbore from each perforation cluster. Away from the wellbore, fluid may or may not divert from the hydraulic fractures into permeable fractures. The strength of this leakoff will depend on the density of permeable natural fractures in the formation.

Because of these issues, significant uncertainty exists about the stimulation mechanism from plug and perf completions performed in crystalline rock. Numerical modeling tools rely on assumptions about stimulation mechanism and the interactions between newly forming and preexisting fractures. Until we have more data, numerical modeling approaches will be affected by this uncertainty. As long as we calibrate models to field data, we can expect them to be reasonably predictive. But clearly, there is a need for direct observations at offset wells to help characterize the far-field fracture geometries and stimulation mechanisms.

Microseismic observations from Stages 1-3 at Utah FORGE shed some insight into the stimulation geometry, but they also have significant uncertainty. Because of operational challenges, the microseismic array was relatively limited during Stages 1-2, and only operated at full capacity during Stage 3. Generally, Stage 1 appeared to show the most diffuse microseismic cloud; Stage 2 showed a moderately diffuse microseismic cloud; and Stage 3 showed a planar microseismic cloud with one apparent bifurcation (Figure 2; McLennan et al., 2023; Pankow, 2023). Possibly, the increasing planarity of the microseismic from Stage 1 to 3 is an indication of the improving quality of the microseismic array. On the other hand, Stage 1 injected into openhole, while Stages 2-3 injected into cased and perforated intervals. Both Stages 1 and 2 used slickwater, while Stage 3 used a crosslinked gel. These operational differences might also be expected to lead to an increasingly planar hydraulic fracturing geometry. Thus, it is ambiguous whether the differences in microseismic observations were caused by operational differences or changes in the microseismic array over time. As additional stages are stimulated at Utah FORGE in the future, and measurements become available from the upcoming 16B(78)-32 offset well, we will gain additional information.

1.2 Technical issues addressed in this paper

In this paper, I apply a planar fracturing model to simulate the stimulation of Stage 3 from Well 16A(78)-32 at the Utah FORGE project (McLennan et al., 2023). The planar fracturing model assumes a single fracture that propagates 'in-plane' without turning. Fluid may be leaking off into natural fractures from this planar fracture, but they are not explicitly represented with a discrete fracture network (DFN) in the model. With future data collection at Utah FORGE, we will resolve ambiguity about fracture morphology, and develop better insights into how often a 'planar' fracture is appropriate, or whether we need to introduce preexisting fractures with a 'DFN' approach. But at least, for Stage 3, the microseismic suggests a planar feature, and so it is reasonable to model this feature with a planar fracturing model. For comparison, Xing et al. (2022) provide an example of a DFN-style model applied to the Utah FORGE system.

Fracture geometry in planar fracture models is affected by a tradeoff between toughness, viscous pressure drop along the fracture, and leakoff (Dontsov and Suarez-Rivera, 2020). If viscous pressure drop is relatively strong (implying either lower conductivity or greater viscosity), then fractures tend to be more symmetrical. If toughness is more dominant, then fracture geometries tend to be driven by stress layering and stress shadowing between adjacent fractures.

In shale, fracture height growth is strongly affected by stress layering caused by differences rock properties between layers (Zoback et al., 2022). However, in the granitic rock of the reservoir at the Utah FORGE project, there is not any 'layering' from sedimentary processes, and the formation should be relatively homogeneous. However, observations show that the formation is not entirely homogeneous; Jones et al. (2021) reports on a cuttings analysis where they observed variations in lithology between granitic and gneissic materials during the drilling of the lateral.

In absence of any stress layering, hydraulic fracturing theory suggests that fractures should tend to grow upwards. At Utah FORGE, the frac gradient has been estimated to be 0.73 psi/ft (Xing et al., 2022). Within a hydraulic fracture during propagation, the pore pressure gradient will typically be hydrostatic, around 0.43 psi/ft. As the fracture grows upwards, the stress decreases more rapidly than the pore pressure. As the fracture grows downwards, the stress increases more rapidly than pore pressure. Thus, since the frac gradient is greater than the pore pressure, there is an upward tendency for propagation.

The microseismic data from Utah FORGE Stage 3 suggests a mostly circular crack with slightly upward propagation (Figure 2). This paper asks – what parameters must be used in a hydraulic fracturing simulator to match these observations?

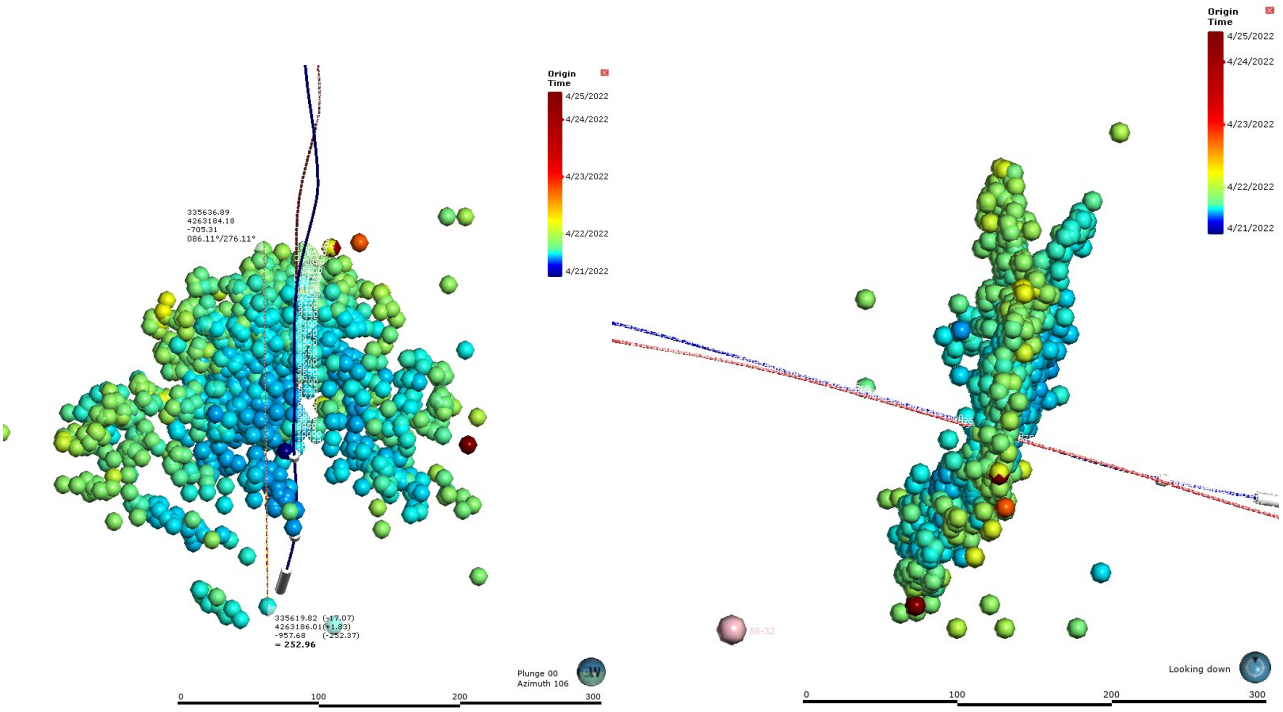

Figure 2: Microseismicity created by the Stage 3 stimulation of 16A(78)-32. Figure courtesy of Ghanashyam Neupane. For the original reference, refer to Pankow (2023).

1.3 Details of Utah FORGE Stage 3

The Stage 3 injection was performed with a crosslinked gel that has significant apparent viscosity over substantial time at ambient temperature, but which degrades rapidly with exposure to reservoir temperature. There was a single perforation 'cluster' consisting of a section of 120 perf shots over 20 ft. The injection pressures and rates are shown in Figure 3. Injection rate was stepped up to a maximum of 35 bpm, held at a plateau, and then stepped back down to zero.

The injection pressure shows an anomalous behavior – peaking near 7200 psi wellhead pressure (WHP) early during the injection (before reaching max rate), and then steadily decreasing through the duration of the job. WHP was about 5150 psi at the end of the 35 bpm period of injection, and reached as low as 3900 psi at the end of injection (at the lowest rate step of 5 bpm). The instantaneous shut-in pressure (ISIP) was around 3600 psi, and pressure decayed to about 3100 psi within 30 min of shut-in. The stage was at around 8500 ft of TVD (true vertical depth), and so assuming hydrostatic head, the implied bottomhole pressure (BHP) at the perforation cluster at the ISIP was 7280 psi (0.856 psi/ft). As discussed in Section 2.3 below, the WHP trend was matched by assuming a near-wellbore tortuosity pressure drop that gradually decreased over the course of injection.

The injection was performed with a microproppant, which was modeled in the simulator as being a 400 mesh proppant. The microproppant concentration versus time is shown in Figure 4. It is not known whether the microproppant influenced the fracture geometry and/or leakoff behavior of the system.

As shown in Figure 2, the microseismic cloud was about 820 ft top to bottom and about 950 ft in lateral extent (Ghanashyam Neupane, personal communication; Pankow, 2023). The aerial view suggests a crack bifurcation on one side (right hand panel of Figure 2). This was not included in the simulation, which assumed a single planar fracture.

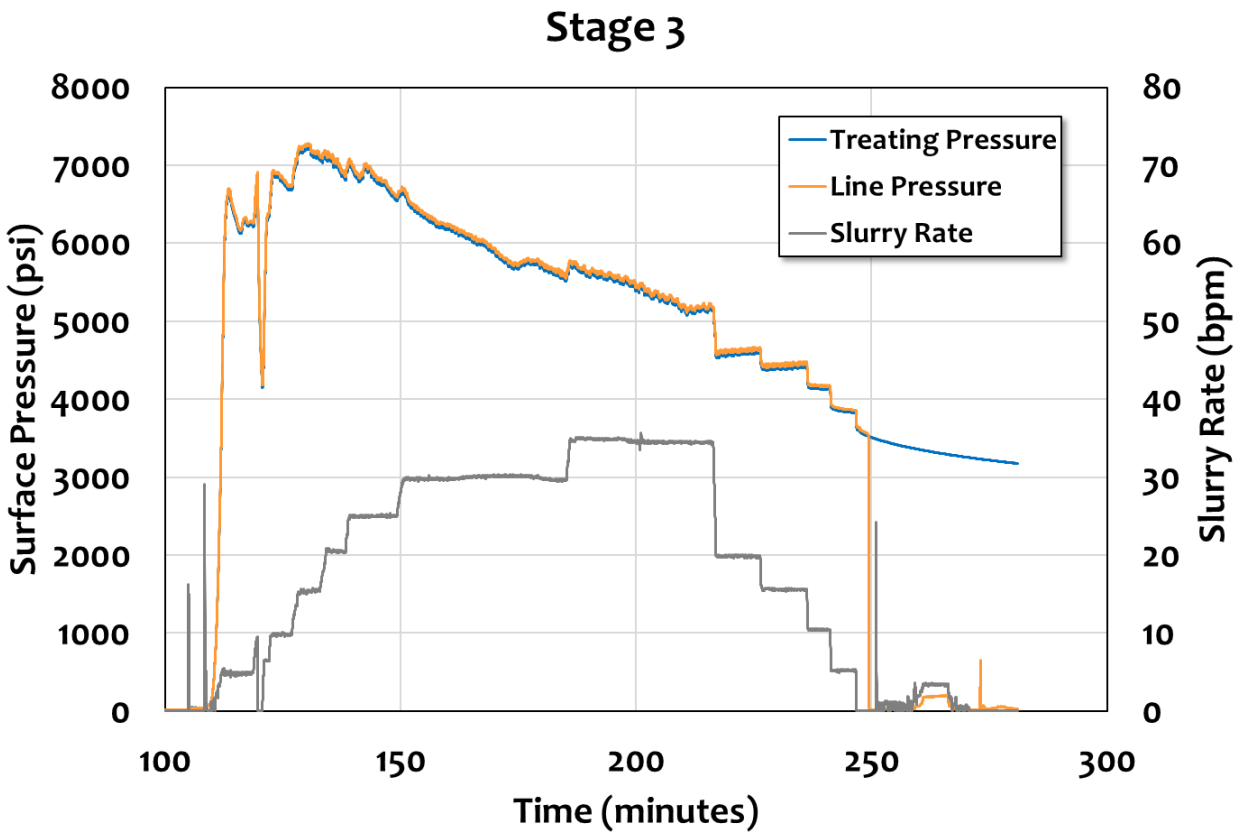

Figure 3: Injection rate and pressure versus time during the 16A(78)-32 Stage 3 injection. Figure courtesy of John McLennan.

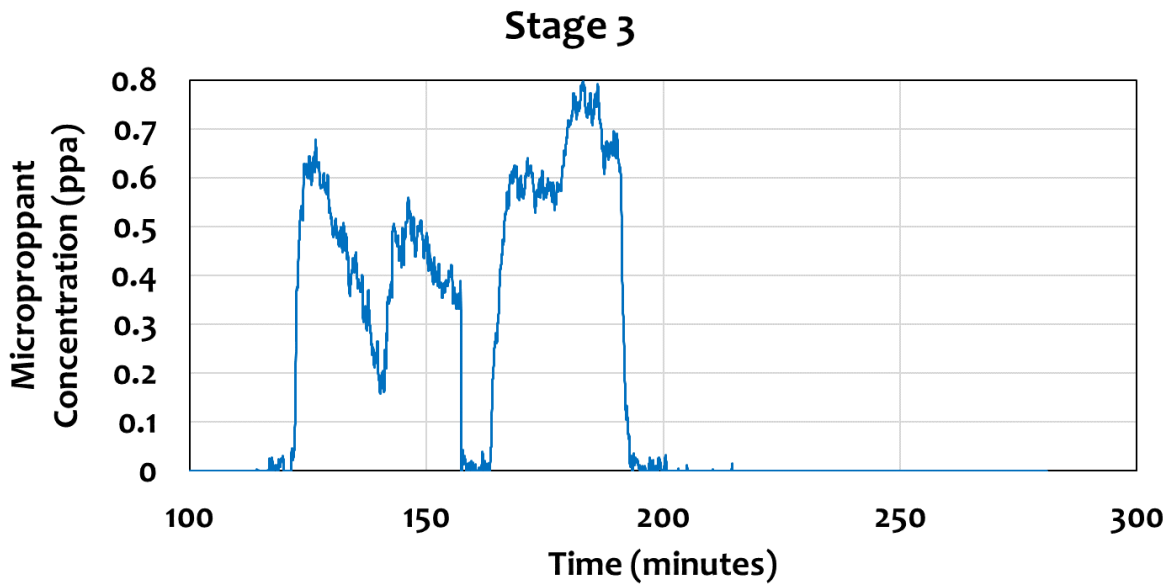

Figure 4: Microproppant concentration versus time during the 16A(78)-32 Stage 3 injection. Figure courtesy of John McLennan.

2. METHODS

2.1 Overall simulation setup

Simulations were performed with ResFrac, an integrated hydraulic fracturing, reservoir, and wellbore simulator (McClure et al., 2022a). The simulator simultaneously solves balance equations on fluid components, proppants, water solutes, and energy, in the fracture, matrix, and wellbore elements. The wellbore is meshed to the surface, and the calculations in the well include momentum balance and the effect of heat conduction with the surrounding formation all the way to the surface. Fracture elements are meshed with rectangular elements; however, the crack tip is tracked 'within' edge elements, allowing for curved fracture fronts and high resolution with respect to formation layering (Dontsov et al., 2022). The matrix is meshed with a rectilinear grid. The grid used in the simulations for this paper is shown in Figure 5. The grid is logarithmically refined perpendicular to the fracture, down to a minimum size of 0.1 ft.

Stresses induced by fracture opening are calculated with the 3D displacement discontinuity method (Shou et al., 1997). The porothermoelastic stress changes induced by pressure and temperature changes are calculated with a finite volume method.

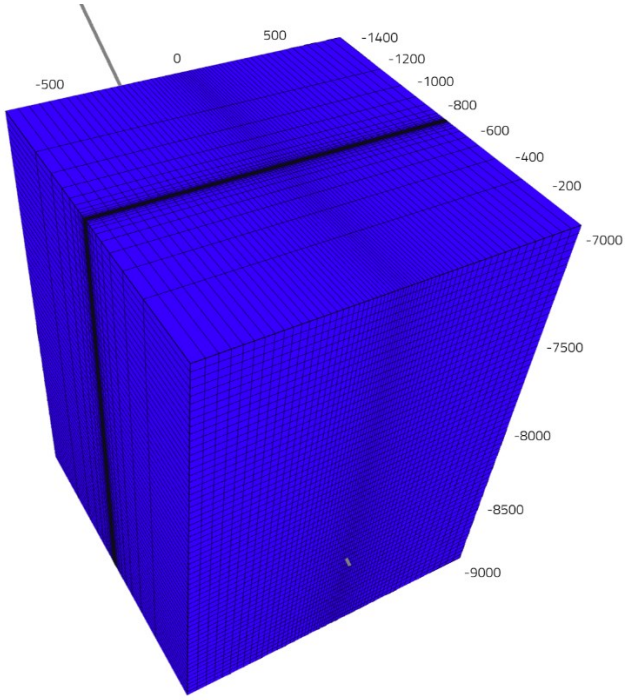

Figure 5: Simulation grid used in the simulations for this paper. The mesh is heavily refined perpendicular to the fractures.

Table 1 summarizes the formation properties used in the simulation. Xing et al. (2022) was used as the primary source for the input parameters. In some cases, if data was not available, reasonable values for a granitic formation were assumed.

Table 1: Input parameters used in the simulations

Permeability (assumed isotropic)	1 microdarcy	Formation compressibility	1e-5 psi^{-1}
Porosity	1%	Fracture gradient	0.73 psi/ft
Rock density	156 lbs/ft^3	Rock heat capacity	0.239 BTU/(lb-R)
Thermal conductivity	1.445 BTU/(hr-ft-R)	Coefficient of linear expansion	5.56e-6 F^{-1}
Biot coefficient	0.35	Horizontal fracture toughness	2740 $psi\text{-}in^{1/2}$
Pore pressure gradient	0.41 psi/ft	Young's modulus	8e6 psi
Poisson's ratio	0.26	Surface temperature	68°F
Thermal gradient	0.033 F/ft	Crosslinked gel viscosity	70 cp at 170 s^{-1} and reservoir temperature
Crosslinked gel decay rate constant	0.67 $hours^{-1}$	Proppant grain diameter	400 mesh

The water properties are calculated as a function of temperature and pressure using high accuracy correlations from the IAPWS. At the initial reservoir temperature and pressure, the water viscosity is around 0.165 cp, and the water density is around 57 lbs/ft^3 (913 kg/m^3).

The automated history match to the fracture geometry was performed using the algorithm described by Kang et al. (2022).

Proppant transport in the simulator includes a phenomenon called 'proppant trapping,' or 'localized screenout' (Maity and Ciezobka, 2020; McClure et al., 2020). The idea is that some proppant is held-up in the fracture by roughness. This reduces total distance that proppant can travel, but also improves vertical proppant placement. In the simulations, the 'maximum immobilized proppant' (as described by McClure et al. 2022a) was set to 0.15 lb/ft^2.

2.2 Field-scale calibration parameters

As discussed above, fracture toughness, viscous pressure drop, and leakoff have a strong effect on fracture geometry (Dontsov and Suarez-Rivera, 2020). These three factors are affected by 'field-scale' processes and require field-scale calibration. For example, if a single apparent 'hydraulic fracture' is actually a swarm of simultaneously propagating fractures (as has been observed in core in shale), then the apparent toughness, viscous pressure drop, and leakoff will all be elevated (Fu et al., 2020). More generally, core-through studies show that even if a fracture appears broadly planar at field-scale, it very likely has significant small-scale complexity and nonplanarity at the scale of inches to feet (Gale et al., 2022). From practical experience, scale-dependent apparent fracture toughness is commonly observed in practical hydraulic fracturing (Shylapobersky, 1986; Section 6-7.2 from Mack and Warpinski, 2000).

In ResFrac, we parameterize elevated field-scale toughness using a 'relative fracture toughness scaling parameter,' such that (Delaney et al., 1986; Scholz, 2010):

$$K_{Ic,eff} = K_{Ic,base}(1 + K_{Ic,fac}\sqrt{l_{ref}}), \quad (1)$$

where $K_{Ic,eff}$ is the effective fracture toughness, $K_{Ic,base}$ is the specified base fracture toughness (equivalent to a value that would be measured in the lab), l_{ref} is the smaller of either the fracture height or length, and $K_{Ic,fac}$ is a scaling factor.

In ResFrac, we parameterize elevated field-scale viscous pressure drop by modifying the cubic law used to calculate conductivity of a mechanically open fracture:

$$C = \frac{(WW_{fac})^3}{12}, \quad (2)$$

where W is the crack aperture, W_{fac} is a factor less than or equal to 1.0, and C is the fracture conductivity. If we specify W_{fac} less than 1.0, this effective reduces the crack aperture available for flow, resulting in a lower fracture conductivity, and greater viscous pressure drop.

Finally, we parameterize elevated field-scale leakoff by defining reversible 'pressure dependent permeability' according to the relation:

$$k = k_{base} \; if \; P < P_{PDP,lower}$$

$$k = k_{base} + (k_{PDP} - k_{base}) \frac{P - P_{PDP,lower}}{P_{PDP,upper} - P_{PDP,lower}} \quad if \; P_{PDP,lower} < P < P_{PDP,upper} \tag{3}$$

$$k = k_{PDP} \; if \; P > P_{PDP,upper}$$

Elevated pressure-dependent permeability (PDP) represents either: (a) pressurization (and unloading) of natural fractures, enhancing leakoff, (b) pressure/stress dependent permeability in the rock matrix (probably not significant for applications in granitic rock), or (c) the effect of closely spaced fracture strands, which elevates the fracture area available for leakoff. In all the simulations run in this paper, $P_{PDP,lower}$ is set 800 psi above initial pressure, $P_{PDP,upper}$ is set 1200 psi above initial pressure.

The user may choose to increase the vertical fracture toughness to be greater than the horizontal fracture toughness. In addition, the user may choose to make the vertical conductivity during propagation lower than the horizontal conductivity, using a parameter $C_{open,fac}$. For example, if $C_{open,fac}$ is set to 0.5, then the vertical conductivity during propagation is set to be 50% lower than the horizontal conductivity. In typical shale applications, it is not uncommon to introduce moderate anisotropy in toughness or conductivity to reduce height growth.

In shale, anisotropy of toughness and conductivity may be rationalized as being caused by layering in the formation (Fu et al., 2019). As noted above, cuttings analysis from Jones et al. (2021) suggested that the formation around 16A(78)-32 has lithologic variability. Possibly, this variability could be responsible for any apparent anisotropy. Speculatively, two other possibilities are: (a) interaction with dipping natural fractures, or (b) anisotropy in flow/propagation properties induced by the anisotropic stress state.

The simulations in this simulation assumed that the formation moduli are isotropic. Speculatively, it is possible that anisotropy of modulus could have affected the aspect ratio of the Stage 3 fracture (Sesetty et al., 2018). Granitic formations are not expected to be highly anisotropic, but nevertheless, this topic deserves further investigation.

2.3 Near-wellbore pressure drop

There are two primary sources of pressure drop between the well and the far-field fracture: (a) perforation pressure drop, and (b) near-wellbore pressure drop caused by tortuosity.

Perforation pressure drop is very important in limited-entry plug and perf completion (Cramer, 1987; Lorwongngam et al., 2020), and was included in the simulations for this paper. However, in the Utah FORGE Stage 3, a very large number of perforation shots were used as part of a single cluster. It is unclear how many of the shots took fluid, but given the high number of shots, it is likely that perforation pressure drop had a negligible effect.

Near-wellbore pressure drop is caused by the tortuous pathway that occurs between the wellbore and the far-field fracture (Wright, 2000; Bazan and Meyer, 2015). When a well is drilled in the direction of Shmin, the far-field fracture will orient perpendicular to the well orientation. However, in the immediate vicinity of the wellbore, the crack may initiate longitudinally along the well, or from natural fractures. The rock around the perforation tunnels is compacted and may be higher stress. Thus, the fluid may need to flow through the annular region containing the cement sheath around the casing to reach the formation and break it down. These processes can cause large pressure drop in the near-wellbore region.

The simulator models near-wellbore pressure drop with the equation (Wright, 2000):

$$\Delta P_{nw} = A_{nw} Q^{0.5} \tag{4}$$

Where ΔP_{nw} is an additional pressure drop between the well and adjacent fracture element(s), A_{nw} is a coefficient, and Q is the volumetric flow rate between the well and adjacent fracture element(s).

Near-wellbore pressure drop can be very large (1000s of psi). In a comparison of 62 diagnostic fracture injection tests in shale, McClure et al. (2022b) found that the near-wellbore pressure drop in horizontal wells varied from 500 psi to more than 6000 psi.

In the Utah FORGE Stage 3 stimulation, injection bottomhole pressure was initially much higher than the minimum principal stress. The injection pressure continuously decreased during injection, dropping several thousand psi, even when injection rate was being stepped up (Figure 3). The net pressure of a single fracture could not possibly be 1000s of psi; this would imply astronomically high fracture toughness. Instead, the elevated injection pressure is being caused by near-wellbore tortuosity. The decreasing injection pressure over time is because caused by a gradual reduction in near-wellbore tortuosity as the well-to-fracture flow pathway opens up due to fluid flow, thermal contraction due to cooling, and possibly due to erosion from the microproppant.

The reduction in near-wellbore tortuosity during injection is modeled with the equation:

$$A_{nw} = A_{nw,init} * 2^{-V_{fl}/V_{fl,nwfac}} \tag{5}$$

Where $A_{nw,init}$ is the initial value of A_{nw}, V_{fl} is the cumulative volume of fluid that has flowed from a particular wellbore element to a particular fracture element, and $V_{fl,nwfac}$ is a normalizing constant. For every $V_{fl,nwfac}$ volume of fluid that flows through the connection, the value of A_{nw} reduces by half.

In the simulations for this paper, $A_{nw,init}$ was set to 839 psi/(bpm)$^{0.5}$, and $V_{fl,nwfac}$ was set to 7500 barrels. As shown in Section 3, these values yield a good match with the observed WHP.

2.4 Specifics of the simulations

The 'Base' simulation is the 'best-match' simulation from the automated history match. For sensitivity analysis, three additional simulations are discussed: (a) a 'Slickwater' simulation that uses slickwater instead of cross-linked gel (lower viscosity frac fluid), (b) an 'Unadjusted Toughness and Conductivity' simulation, and (c) an 'Unadjusted Toughness and Conductivity with No PDP' simulation. Table 2 summarizes the differences between the simulations.

Laboratory testing showed that the crosslinked gel should degrade over a period of a few hours. To represent this in the simulation, a reaction was defined so that the crosslink would degrade into linear gel over a similar time period.

Table 2: Differences between input parameters in different simulations

Property	Base	Slickwater	Unadjusted Toughness & Conductivity	Unadjusted Toughness & Conductivity, and No PDP
W_{fac} (adjustment to the effective aperture for conductivity)	0.40	0.40	1.0	1.0
$K_{Ic,fac}$ (scaling of toughness with sqrt fracture size)	0.10 ft$^{-1/2}$	0.10 ft$^{-1/2}$	0 ft$^{-1/2}$	0 ft$^{-1/2}$
k_{PDP} (effective permeability to leakoff)	55.4 μD	55.4 μD	55.4 μD	1 μD
Base vertical toughness	4510 psi-in$^{-1/2}$	4510 psi-in$^{-1/2}$	2740 psi-in$^{-1/2}$	2740 psi-in$^{-1/2}$
$C_{open,fac}$ (reduction factor for vertical conductivity during propagation)	0.60	0.60	1.0	1.0
Frac fluid viscosity at 170 s-1	69.7 cp	0.45 cp	69.7 cp	69.7 cp

All of the simulations use the same injection rate versus time and proppant versus time, reproducing the injection schedule shown in Figure 3 and Figure 4.

3. RESULTS AND DISCUSSION

The upper left panel of Figure 6 shows the injection rate, WHP, BHP, and 'fracture pressure adjacent to the well' versus time for the 'Base' simulation. In the plot, the 'fracture pressure adjacent to the well' is the pressure in the fracture element adjacent to the fracture element on the other side of the 'near-wellbore tortuosity.' The other panels of Figure 6 show pressure, temperature, aperture, proppant mass per area, and fluid viscosity after about two hours of injection. The fracture has a total height of 820 ft, and a total length of 940 ft. The fracture has grown upwards slightly more than it has grown downwards. These geometries are consistent with the distribution of observed microseismic events.

As in the actual data (Figure 3), the simulated injection WHP peaks after about 30 min of injection – as injection rate continues to be stepped up – and then declines by almost 4000 psi by shut-in. As described in Section 2.3, this phenomenon is modeled as near-wellbore tortuosity that erodes over the duration of the stimulation.

The simulated WHP is similar to the actual WHP, with two notable exceptions. First, the injection pressure at early-time – prior to the peak in WHP – is underestimated by the simulation. Second, the simulation predicts a greater drop in WHP in the minutes immediately after shut-in. In the simulation, the WHP quickly drops by about 1000 psi after shut-in. In the actual data, the pressure only drops by about 300 psi immediately after shut-in; then, it continues decreasing fairly rapidly for the remainder of the data shown in Figure 3. The most likely cause of the discrepancy is that – in the actual data – dissipation of the full near-wellbore tortuosity effect continued for an extended

period of after shut-in. As reviewed by McClure et al. (2022b), near-wellbore tortuosity is routinely observed to require tens of minutes or even hours to dissipate. Because near-wellbore tortuosity was substantial during this injection, it is very plausible that it could have persisted for an extended period after shut-in. The near-wellbore tortuosity model defined in Equation 4 tends to dissipate quickly after shut-in and is not able to match periods with extended periods of near-wellbore tortuosity. Section 19.5 from McClure et al. (2022b) describes an alternative model for near-wellbore tortuosity – using a pressure-dependent conductivity barrier – that can better match extended post-shut-in near-wellbore pressure drop.

Near-wellbore pressure drop is not a significant problem for the fracturing treatment because injection pressure can be increased sufficiently to pump the job as designed. However, during long-term circulation, near-wellbore tortuosity could create resistance to flow. Thus, it may be desirable to use operational strategies to reduce tortuosity; for example, an acid spear could be pumped at the start of the treatment.

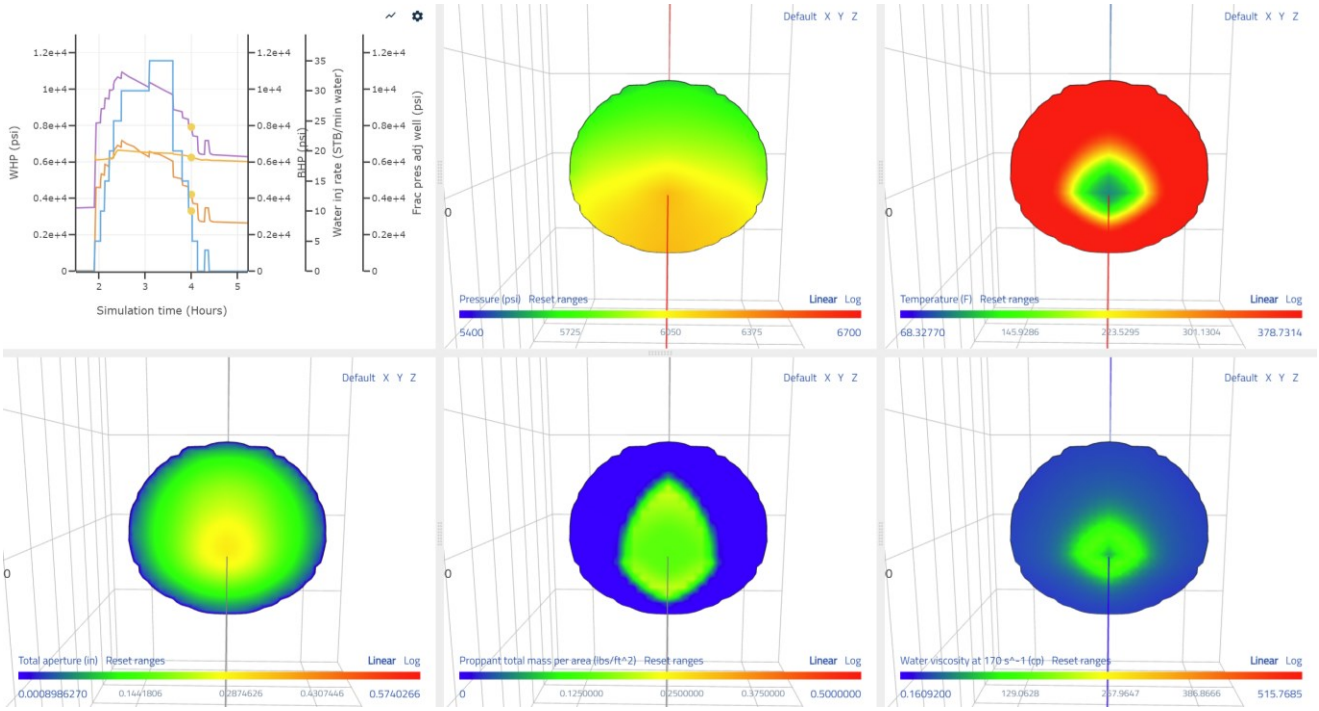

Figure 6: Simulated fracture geometry, injection rate, and pressure after two hours of injection time from the 'Base' simulation.

Figure 7 shows the distribution of pressure, temperature, and thermoporoelastic stress changes in the matrix around the fracture at the end of shut-in. The region of pressure increase around the fracture (upper left panel) is much wider than the region of cooling, which forms a very thin, barely-visible line around the fracture (upper right panel). Consequently, the poroelastic stress increase is stronger than the thermoelastic stress decrease, and the net effect is an increase in the compressive stress of around 150 psi. Above and below the fracture and zone of pressure increase, there is a modest decrease in stress; this arises from the solution to the 3D deformation equations. As the

rock around the fracture expands from pressure increase, the surrounding rock must deform in response to maintain compatibility, and this creates localized stress decrease above and below.

The zone of cooling within the fracture has a diameter of roughly 280 ft. However, because the region of cooling in the formation perpendicular to the fracture is so thin, it reheats rapidly after shut-in. Figure 8 shows that after just two hours of shut-in, the fracture has already reheated substantially.

Figure 8 shows that after a few hours of shut-in, the fluid viscosity in the fracture has dropped substantially because of the degradation of the crosslinked gel. The fracture has almost entirely closed mechanically, and the microproppant has been placed in an elliptical region around the well.

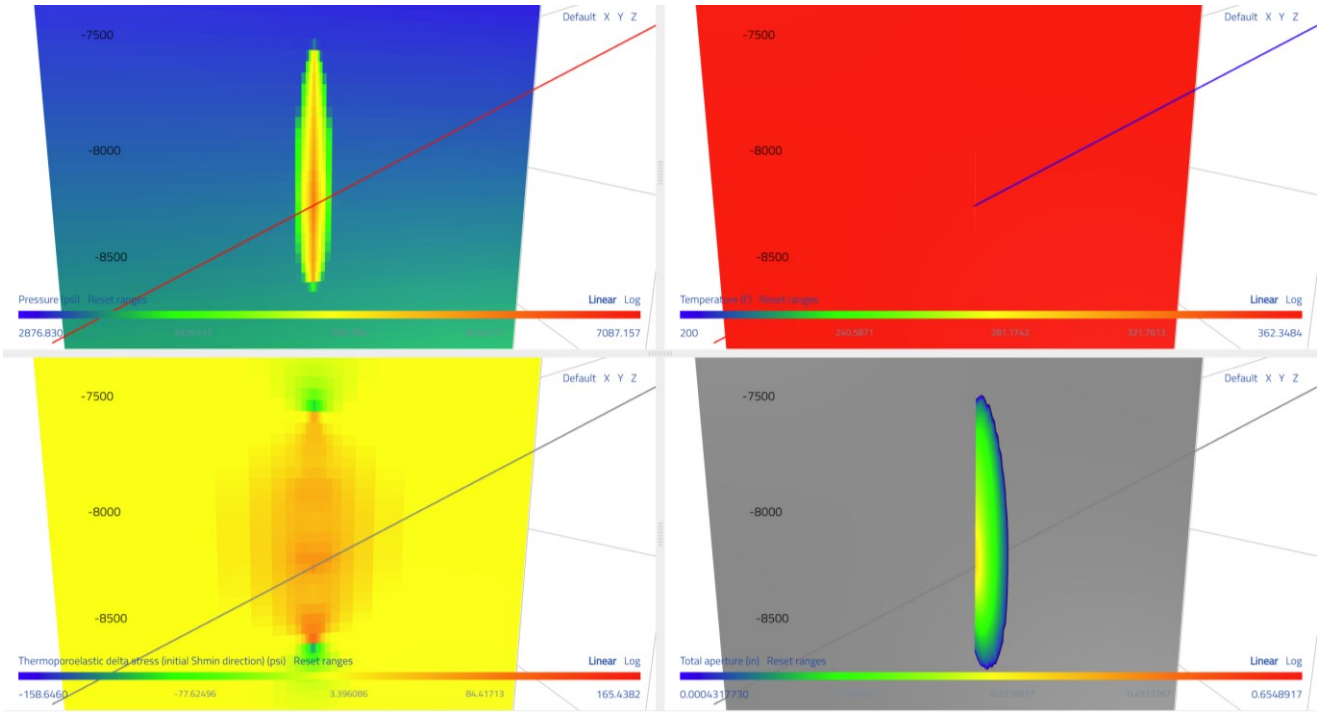

Figure 7: Simulated distribution of pore pressure, temperature, and thermoporoelastic stress change in a cross-section through the matrix. For visibility, the fracture is hidden in three of the panels.

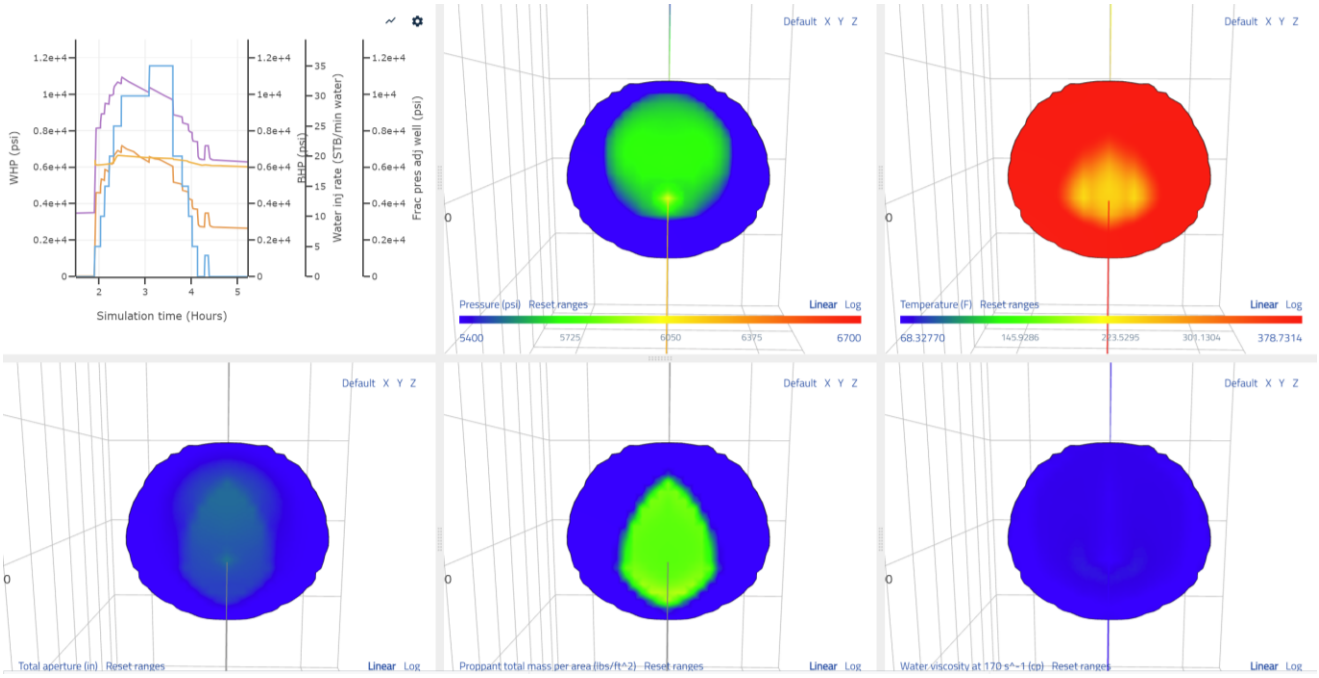

Figure 8: Simulated fracture geometry, injection rate, and pressure two hours after shut-in from the 'Base' simulation.

The automated history matching routine ran a total of 60 simulations, spanning a wide range of input parameters for toughness, conductivity, leakoff, anisotropy of toughness, and anisotropy of conductivity during propagation (Table 2). The 'Base' simulation has the 'best-fitting' combination of parameters. The algorithm did not identify another substantially different combination of parameters that was able to provide a good fit to the target fracture geometry. This suggests that the match was well-constrained (ie, not 'non-unique').

Interestingly, the settings used in the 'Base' simulation were reasonably consistent with the settings that might be used in a typical simulation in shale, such as those described by McClure et al. (2022c). It is common to introduce moderate increase in toughness and decrease in conductivity, to introduce substantial pressure-dependent permeability to accelerate leakoff, and to introduce anisotropy in either toughness or conductivity.

Comparing across the range of simulations run by the algorithm, it was evident that the value of 'PDP multiplier' had to be in the range of 40-60x (implying an effective permeability to leakoff of 40-60 microdarcy), or else the fracture size would be grossly incorrect. Without sufficient leakoff, the fracture would grow far too large, and with excessive leakoff, it would grow too small. Evidently, the elevated pressure in the propagating hydraulic fracture substantially accelerates leakoff into the surrounding natural fractures.

Given the fracture dimensions in the simulation, the $K_{Ic,fac}$ value of 0.10 ft$^{-1/2}$ implies a roughly 4x increase in toughness from the base value. The W_{fac} value of 0.6 results in a 78% reduction in conductivity. Both the toughness and conductivity adjustments affect fracture size, but nevertheless, the match was not nonunique. While simulations with lower conductivity and lower toughness might have similar surface area, they would have different aspect ratio because lower conductivity tends to result in a more circular crack. Conversely, a match with substantially greater toughness and conductivity could have similar surface area, but would have had too much upward growth. Thus, because the history matching objective required a match to both height and length, the effects of $K_{Ic,fac}$ and W_{fac} were separable.

The two anisotropy parameters – vertical toughness and vertical conductivity multiplier – had the effect of roughly doubling the toughness and causing a roughly 40% decrease in vertical conductivity. Without these anisotropy parameters, the fracture would have had greater height than length, rather than the actual observation that the fracture had greater length than height. Looking across the range of 'closest match' simulations, there did appear to be some nonunique tradeoff between these two parameters; higher vertical toughness could be compensated with lower vertical conductivity and vice-versa. The 'best-fit' simulation included a moderate amount of both.

Figure 9 shows the distribution of properties after two hours of injection from the 'Slickwater' simulation. Compared with the 'Base' simulation, which used a much more viscous fluid, the fracture experienced significantly more upward growth. The fracture was both longer and taller - 930 ft total height and 980 ft long at the widest point. The lower viscosity allows the effect of 'decreasing frac gradient with depth' to be more dominant.

This simulation shows hypothetically what the fracture geometry might have looked like if the stage had been pumped with slickwater. However, this cannot be considered a high-confidence prediction. We need more data from more stages, using both slickwater and crosslinked gel, to provide better constraint on the field scale processes controlling hydraulic fracture propagation in the context of a

stimulation design like that used at Utah FORGE. Stage 2 from Utah FORGE was pumped with slickwater, but as discussed above, the microseismic receiving array was different than during Stage 3, and so it cannot necessarily be used as a direct comparison.

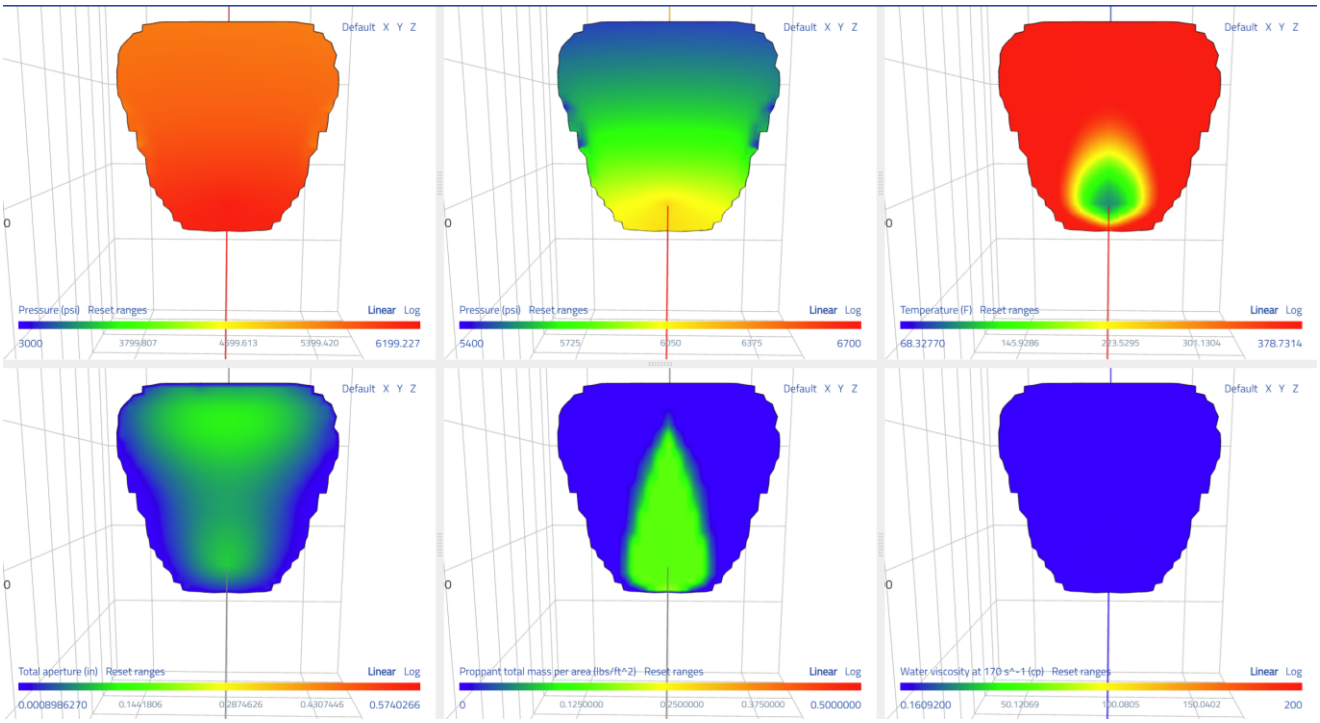

Figure 9: Simulated fracture geometry, injection rate, and pressure after two hours of injection in the 'Slickwater' simulation.

Figure 10 shows the distribution of properties after two hours of injection in the 'Unadjusted Toughness and Conductivity' simulation. This is the simulation where the toughness and conductivity adjustments are not applied, but the PDP increase is still included. The fracture experiences much greater height growth, and now has a much more vertical aspect ratio (1256 ft height and 800 ft length).

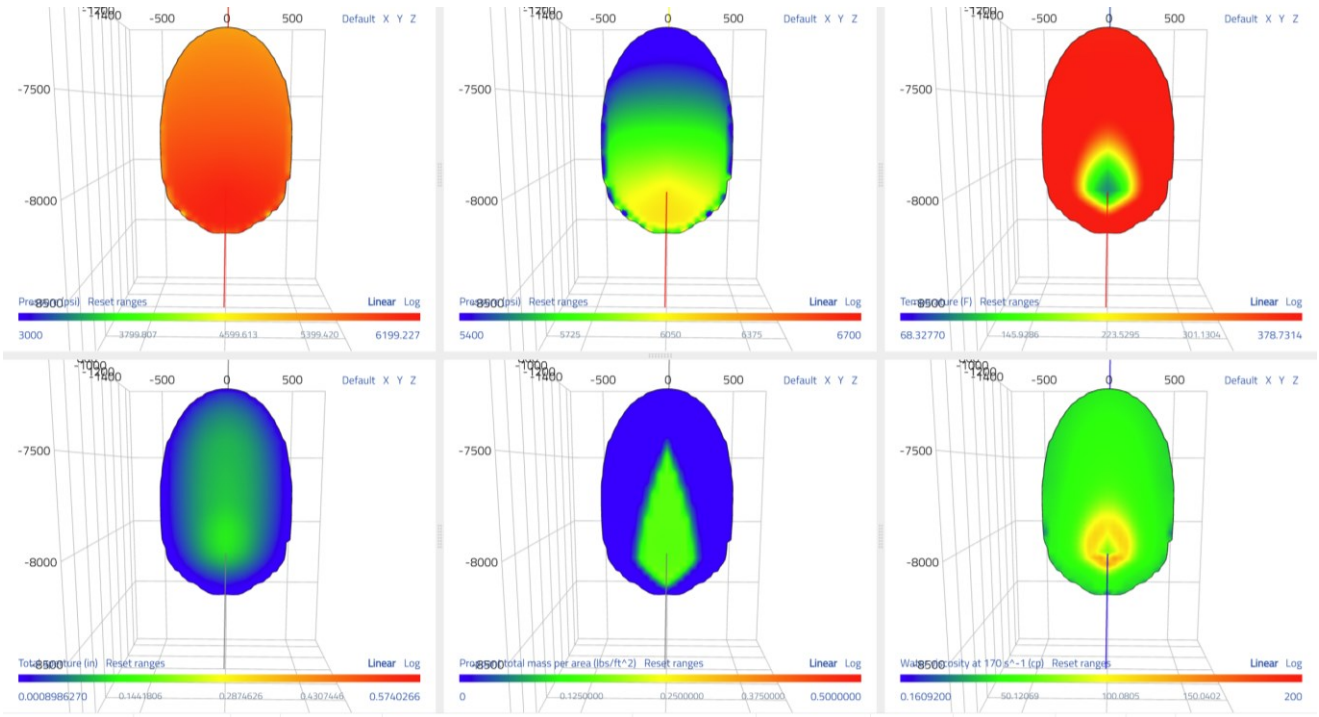

Figure 10: Simulated fracture geometry, injection rate, and pressure after two hours of injection from the 'Unadjusted Toughness and Conductivity' simulation.

Figure 11 shows the distribution of properties after two hours of injection in the 'Unadjusted Toughness and Conductivity and No PDP' simulation. The results of this simulation are grossly unrealistic. The fracture height is 3400 ft, and the fracture length is 940 ft. Without effective permeability for leakoff in the ballpark of 40-60 microdarcy, the fracture surface area is much too large.

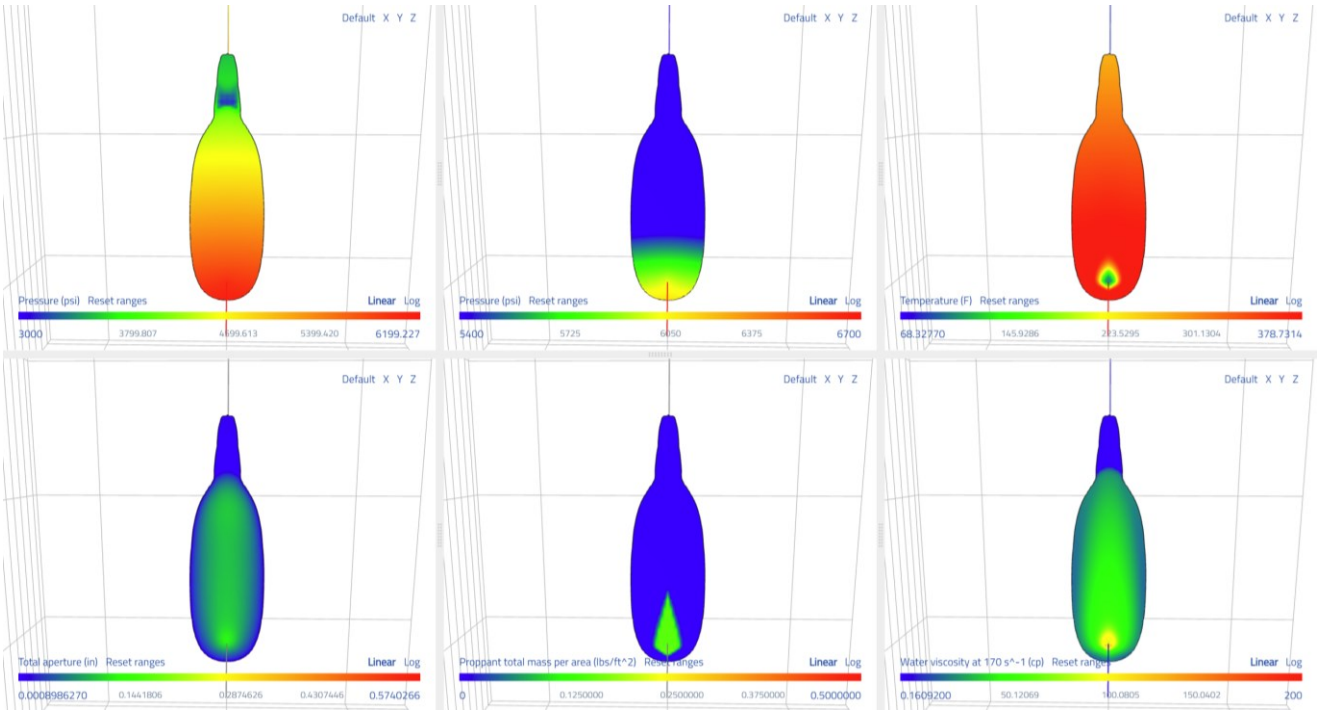

Figure 11: Simulated fracture geometry, injection rate, and pressure after two hours of injection from the 'Unadjusted Toughness and Conductivity and No PDP' simulation.

4. CONCLUSIONS

The results demonstrate that the fracture geometry from the Utah FORGE Well 16A(78)-32 Stage 3 stimulation can be matched with a planar fracture model. However, field-scale calibration parameters must be modified to account for non-ideality and small-scale fracture roughness – these includes modifications to toughness, leakoff, fracture conductivity, and the introduction of anisotropy in conductivity and toughness. The fracture size is constrained primarily by leakoff, but also by toughness and viscous pressure drop. The apparent permeability to leakoff was in the ballpark of 40-60 μD. Viscous pressure drop is the most important process that prevents the fracture from having excessive height growth. In addition, to generate a fracture with greater length than height, it is necessary to assume moderate anisotropy of the toughness and conductivity. A hypothetical simulation with lower-viscosity slickwater fluid had a stronger upward bias in the propagation direction than the 'Base' simulation with crosslinked gel.

Interestingly, the calibration parameters are 'in the ballpark' of what might be used in a field-scale fracturing simulation in shale (McClure et al., 2022c). This may be coincidental because the geologic setting is very different from shale. Elevated leakoff and toughness and reduced conductivity can be rationalized as being caused by interaction with natural fractures and small-scale fracture complexity/non-ideality. It is not as obvious how to rationalize why fracture conductivity and toughness would be anisotropic during stimulation in a granitic rock mass. Nevertheless, the match to the observed fracture geometry would not have been possible without this anisotropy. Considering the variable lithology seen in cuttings by Jones et al. (2021), it is possible that the model setup underestimated the heterogeneity of the rock mass. If the fracture encountered layers of variable lithology as it propagated vertically, this would manifest as anisotropic toughness (Fu et al., 2019).

The Utah FORGE Well 16A(78)-32 Stage 3 stimulation was performed with cross-linked gel and from a single perforated interval. As further data is collected at the FORGE site, it will be interesting to repeat this calibration exercise to observe if the parameters inferred from this experiment are successful at matching geometries from future injections, or if modifications are needed. Future injection may involve additional cluster spacing, different types of fluid, and/or different types of proppant. Ultimately, cross-well circulation with a future well, 16B(78)-32, will yield measurements of the fracture conductivity and flow rate that can be achieved from multistage stimulation for EGS.

ACKNOWLEDGEMENTS

Thank you to John McLennan, Ghanashyam Neupane, Rob Podgorney, and Kevin England for providing the figures and data used in the preparation of this paper. Also, thank you to Ghanashyam Neupane, Joe Moore, John McLennan, and Kevin England for providing helpful comments on the initial draft of the paper. A huge kudos to the Utah FORGE team for their successful execution of the project to-date and to the US Department of Energy Geothermal Technologies Office for their leadership and support.

REFERENCES

Bazan, Lucas W. and Bruce R. Meyer. 2015. Fracture complexity: analysis methodology and signature pressure behavior of hydraulic fracture propagation from horizontal wellbores. SPE 176919. Paper presented at the SPE Asia Pacific Unconventional Resources Conference and Exhibition, Brisbane, Australia.

Cramer, D. D. 1987. The application of limited-entry techniques in massive hydraulic fracturing treatments. Paper SPE 16189-MS presented at the SPE Production Operations Symposium, Oklahoma City, OK.

Delaney, Paul T., David D. Pollard, Joseph I. Ziony, and Edwin H. McKee. 1986. Field relations between dikes and joints: emplacement processes and palesostress analysis. Journal of Geophysical Research 91 (B5): 4920-4938.

Doe, Thomas, and Robert McLaren. 2016. Discrete Fracture Network Analysis of Controlling Factors for EGS Performance. Paper presented at the 41st Workshop on Geothermal Reservoir Engineering, Stanford University.

Dontsov, E. V., and R. Suarez-Rivera. 2020. Propagation of multiple hydraulic fractures in different regimes. International Journal of Rock Mechanics and Mining Sciences 128(104270).

Dontsov, Egor, Christopher Hewson, and Mark McClure. 2022. A new crack propagation algorithm that enables accurate simulation of propagation across thin layers in a practical field-scale fracturing model. Paper SPE 209146-MS presented at the SPE Hydraulic Fracturing Technology Conference, The Woodlands, TX.

Evans, K. F., A. Genter, and J. Sausse. 2005. Permeability creation and damage due to massive fluid injections into granite at 3.5 km at Soultz: 1. Borehole observations, Journal of Geophysical Research, 110(B4).

Fercho, Steven, Jack Norbeck, Emma McConville, Saurabh Agarwal, Sireesh Dadi, Christian Gradl, Nick Hinz, Camden Lang, Aleksei Titov, Katharine Voller, and Timothy Latimer. 2023. Geology, State of Stress, and Heat in Place for a Horizontal Well Geothermal Development Project at Blue Mountain, Nevada. Paper presented at the 48th Workshop on Geothermal Reservoir Engineering, Stanford University.

Fu, Pengcheng, Jixiang Huang, Randolph R. Settgast, Joseph P. Morris, and Frederick J. Ryerson. 2019. Apparent Toughness Anisotropy Induced by Roughness of in Situ Stress: A Mechanism that Hinders Vertical Growth of Hydraulic Fractures and Its Simplified Modeling. Paper SPE-194359-MS presented at the Hydraulic Fracturing Technology Conference and Exhibition, The Woodlands, TX.

Fu, Wei, Joseph Morris, Pengcheng Fu, Jixiang Huang, Chris Sherman, Randolph Settgast, Hui Wu, Frederick Ryerson. 2020. Developing upscaling approach for swarming hydraulic fractures observed at Hydraulic Fracturing Test Site through Multiscale Simulations. Paper SPE-199689-MS presented at the SPE Hydraulic Fracturing Technology Conference and Exhibition, The Woodlands, TX.

Fu, Pengcheng, et al. 2022. Close observations of hydraulic fracturing at EGS Collab Experiment 1: Fracture trajectory, microseismic interpretations, and the role of natural fractures. JGR Solid Earth, 10.1029/2020JB020840.

Gale, Julia Fiona Wells, Sara J. Elliott, Bethany G. Rysak, and Stephen E. Laubach. 2022. The critical role of core in understanding hydraulic fracturing. From: Neal, A., Ashton, M., Williams, L.S., Dee, S.J., Dodd, T.J.H. and Marshall, J.D. (eds) Core Values: the Role of Core in Twenty-first Century Reservoir Characterization. Geological Society, London, Special Publications, 527.

Jones, Clay G., Joseph N. Moore, and Stuart F. Simmons. 2021. X-ray diffraction and petrographic study of cuttings from Utah FORGE Well 16A(78)-32. GRC Transactions 45.

Kang, Charles A., Mark W. McClure, Somasekhar Reddy, Mariyana Naidenova, and Zdravko Tynakov. 2022. Optimizing shale economics with an integrated hydraulic fracturing and reservoir simulator and a Bayesian automated history matching and optimization algorithm. Paper SPE-209169-MS presented at the Hydraulic Fracturing Technology Conference, The Woodlands, TX.

Li, Tianyu, Sogo Shiozawa, and Mark W. McClure. 2016. Thermal breakthrough calculations to optimize design of a multiple-stage Enhanced Geothermal System. Geothermics 64, 455-465.

Lorwongngam, Apiwat (Ohm), Shawn Wright, Stephanie Hari, Erin Butler, Michael McKimmy, Jennifer Wolters, and Craig Cipolla. 2020. Using multidisciplinary data gathering to evaluate eXtreme limited entry completion design and improve perforation cluster efficiency. Paper URTeC-2796 presented at the Unconventional Resources Technology Conference, Austin, TX.

Mack, Mark G., and Norman R. Warpinski. 2000. Mechanics of Hydraulic Fracturing. In Reservoir Stimulation, eds, Michael J. Economides and Kenneth G. Nolte, Wiley.

Maity, Debotyam, and Jordan Ciezobka. 2020. A data analytics framework for cored fracture imaging and novel characterization workflow – application on samples from Hydraulic Fracturing Test Site HFTS in the Midland Basin. SPE-199725-MS. Paper presented at the SPE Hydraulic Fracturing Technology Conference and Exhibition, The Woodlands, TX.

McClure, Mark W., Roland N. Horne. 2014. An Investigation of Stimulation Mechanism in Enhanced Geothermal Systems. International Journal for Rock Mechanics and Mining Sciences 72: 242-260.

McClure, Mark. Matteo Picone, Garrett Fowler, Dave Ratcliff, Charles Kang, Soma Medam, and Joe Frantz. 2020. Nuances and frequently asked questions in field-scale hydraulic fracture modeling. SPE-199726-MS. Paper presented at the SPE Hydraulic Fracturing Technology Conference and Exhibition, The Woodlands, TX.

McClure, M., Kang, C., Hewson, C., Medam, S., Dontsov, E., and Singh, A. (2022a). ResFrac Technical Writeup. http://arxiv.org/abs/1804.02092.

McClure, Mark, Garrett Fowler, Matteo Picone. 2022b. Best practices in DFIT interpretation: Comparative analysis of 62 DFITs from nine different shale plays. Paper SPE-205297-MS presented at the SPE International Hydraulic Fracturing Technology Conference and Exhibition, Muscat, Oman.

McClure, Mark, Magdalene Albrecht, Carl Bernet, Kenneth Etcheverry, Aaron Fuhr, Amin Gherabati, Claudia Molina, Christopher Ponners, Dave Ratcliff, Janz Rondon, Rohit Sinha, Anthony Sung, Jian Xu. 2022c. Results from a Collaborative Parent/Child Industry Study: Permian Basin. Paper SPE-211899-MS presented at the SPE Permian Basin Energy Conference, Midland, TX.

McLennan, J., England, K., Rose, P., Moore, J., and Barker, B. 2023. Stimulation of a High-Temperature Granitic Reservoir at the Utah FORGE Site. Presented at the SPE Hydraulic Fracturing Technology Conference and Exhibition, The Woodlands, TX.

Moore, J., McLennan, J., Allis, R., Pankow, K., Simmons, S., Podgorney, R., Wannamaker, P., Bartley, J., Jones, C., Rickard, W. 2019. The Utah Frontier Observatory for Research in Geothermal Energy (FORGE): An International Laboratory for Enhanced Geothermal System Technology Development. Proceedings of the 44th Workshop on Geothermal Reservoir Engineering, Stanford University.

Norbeck, Jack, Christian Gradl, Saurabh Agarwal, Sireesh Dadi, Steven Fercho, Camden Lang, Emma McConville, Aleksei Titov, Katharine Voller, and Timothy Latimer. 2023. Drilling and Completions Engineering Review of a Horizontal Geothermal Drilling Program and a Multistage, Multicluster Hydraulic Stimulation Treatment Design at Blue Mountain, Nevada. Paper presented at the 48th Workshop on Geothermal Reservoir Engineering, Stanford University.

Pankow, Kristine. Utah FORGE Seismic Events Related to the April, 2022 Well 16A(78)-32 Stimulation. United States: N.p., 09 Nov, 2022. Web. doi: 10.15121/1908927.

Raterman, Kevin T., Yongshe Liu, and Logan Warren. 2019. Analysis of a drained rock volume: An Eagle Ford example. Paper URTeC-2019-263 presented at the Unconventional Resources Technology Conference, Denver, CO.

Samuel, Abraham, William M. Rickard, Ernesto Rivas, Sami Atalay, Joseph Moore, Jordan Self, Matt Stevenson. 2022. Improvement in rate of penetration in FORGE drilling through real time MSE analysis and improved PDC technology. Proceedings, 47th Workshop on Geothermal Reservoir Engineering, Stanford University.

Scholz, Christopher H. 2010. A note on the scaling relations for opening mode fractures in rock. Journal of Structural Geology 32: 1485-1487.

Sesetty, Varahanaresh, Ahmad Ghassemi, Ivan Gil. 2018. An integrated field and numerical study of the impact of formation anisotropy on stage spacing on horizontal wells. Paper URTeC-2878152 presented at the Unconventional Resources Technology Conference, Houston, TX.

Shou, Keh-Jian, Eduard Siebrits, Steven L. Crouch. 1997. A higher order displacement discontinuity method for three-dimensional elastostatic problems. International Journal of Rock Mechanics and Mining Sciences 34 (2): 317-322.

Shylapobersky, J. 1985. Energy analysis of hydraulic fracturing. Paper presented at the 26th US Symposium on Rock Mechanics, Rapid City, South Dakota.

Ugueto, Gustavo A., Magdalena Wojtaszek, Paul T. Huckabee, Alexei A. Savitski, Artur Guzik, Ge Jin, J. Andres Chavarria, Kyle Haustveit. 2021. An integrated view of hydraulic induced fracture geometry in Hydraulic Fracture Test Site 2. Paper URTeC: 5396 presented at the Unconventional Resources Technology Conference, Houston, TX.

Weng, X., O. Kresse, C.-E. Cohen, R. Wu, and H. Gu. 2011. Modeling of hydraulic-fracture-network propagation in a naturally fractured formation. SPE Production & Operations, 26(4).

Wright, Chris. 2000. Section 9E: Rate step-down test analysis – a diagnostic for fracture entry. In Reservoir Stimulation, eds, Michael J. Economides and Kenneth G. Nolte, Wiley.

Xing, Pengju, Duane Winkler, Leroy Swearingen, Joseph Moore, and John McLennan. 2021. In-situ stresses and permeability measurements from testings in Injection Well 16A(78)-32 at Utah FORGE site. GRC Transactions 45: 871-884.

Xing, Pengju, Branko Damjanac, Zorica Radakovic-Guzina, Maurilio Torres, Aleta Finnila, Robert Podgorney, Joseph Moore, and John McLennan. 2022. Numerical simulation of stimulations at the Utah FORGE site using the designed pumping schedules. GRC Transactions 46: 618-628.

Zoback, Mark, Troy Ruths, Mark McClure, Ankush Singh, Arjun Kohli, Brendon Hall, Rohan Irvin, and Malcolm Kintzing. 2022. Lithologically-controlled variations of the least principal stress with depth and resultant frac fingerprints during multi-stage hydraulic fracturing. Paper URTeC-3722883 presented at the Unconventional Resources Technology Conference, Houston, TX.